Mao *et al.*
Chinese Journal of Mechanical Engineering (2024) 37:3
https://doi.org/10.1186/s10033-023-00986-3

Chinese Journal of Mechanical Engineering

ORIGINAL ARTICLE

Open Access

Nonlinear Impact Damage Evolution of Charpy Type and Analysis of Its Key Influencing Factors

Jianfeng Mao[1,2*], Qian Xu[1], Jiadong Yang[1], Chi Cao[1], Dasheng Wang[3], Fengping Zhong[4] and Mingya Chen[5]

Abstract

The current research of Charpy impact mainly focuses on obtaining the ductile brittle transition temperature of materials by experiments. Compared with experiments, numerical simulation can study many problems with harsh conditions. However, there are still few studies on the influence of geometric factors such as side grooves. In this paper, the geometry of standard Charpy impact test is designed. Specimens with different widths and side grooves are tested. The finite element model of Charpy impact was established by ABAQUS software. Use test results and simulation results to verify each other. The effects of sample width, side groove depth and side groove bottom fillet on the impact fracture resistance of the sample were studied. The results show that the specimen width is positively correlated with the impact toughness of the specimen. The side groove greatly reduces the impact toughness of the material; the toughness of side groove decreases with the increase of depth; the fracture toughness of side groove decreases with the increase of fillet at the bottom of side groove. The proportion of toughness energy to impact energy of samples was analyzed. The results show that the toughness energy accounts for about 70% of the impact energy of the sample, which has little to do with the geometric characteristics of the sample. This study presents a reliable method for studying Charpy impact tests. The influence of geometric parameters is obtained, which provides a reference method for the study of impact toughness of high toughness materials.

Keywords Johnson-Cook model, Impact toughness, Charpy impact

1 Introduction

Reactor pressure vessels (RPV) are pressure-bearing special equipments, which plays an irreplaceable role in nuclear power plant [1]. RPV in operation may suffer creep, creep fatigue, fracture and other forms of failure [2–4]. When there is an uncertain dynamic shock load, the pressure vessel is prone to the risk of explosion. Therefore, RPV not only has enough strength, but also has enough toughness [5–7]. Charpy impact test is one of the most important tests to study impact toughness due to its simplicity and rapidity. It can be used to explain the mechanism of impact fracture process, and Charpy impact tester can be used to obtain the load-displacement curve during the impact fracture process. In the fracture simulation of ductile metal at high strain rates, the Johnson-Cook model [8] has a relatively clear physical significance, and is relatively easy to obtain, so it has been widely used.

In the past 20 years, the Charpy impact test method has been further supplemented and improved in many

*Correspondence:
Jianfeng Mao
maojianfeng@zjut.edu.cn
[1] Institute of Process Equipment and Control Engineering, Zhejiang University of Technology, Hangzhou 310032, China
[2] Taizhou Key Laboratory of Advanced Manufacturing Technology, Taizhou Institute, Zhejiang University of Technology, Taizhou 318014, China
[3] State Key Laboratory of Nuclear Power Safety Monitoring Technology and Equipment, Shenzhen 518172, China
[4] Zhejiang Academy of Special Equipment Science, Hangzhou 310020, China
[5] Suzhou Nuclear Power Research Institute, Suzhou 215004, China

aspects such as sample size, shape and size of pendulum hammer blade [9]. The rationality and scientificity of the test have been greatly strengthened. Terán et al. [10] studied the impact toughness of materials at different locations along the processing direction. The results show that the Charpy impact energy is related to the rolling direction. Most of the existing testing machines can only measure Charpy impact energy below 450 J. Therefore, many researchers have come up with many schemes to measure the high impact energy, such as adding side grooves to the sample. Gioacchino et al. [11], Lucon [12] and Al-Jabr et al. [13] experimentally demonstrated that Charpy impact specimens with side grooves significantly reduce the impact energy of the material. The side grooves can eliminate the influence of shear lip on impact energy, and also eliminate the influence of material transverse expansion, consequently determining the crack initiation time [14, 15].

In addition to test methods, there are also many research methods on numerical simulation. The J-C model parameters of typical armored steel are determined through experiments, and the impact behaviors are simulated by this model, and the simulation results are consistent with the test [16]. Cao et al. [17] provided J-C model parameters of X80 pipeline steel, and studied the effects of sample width and impact velocity on fracture behaviours. Gambirasio et al. [18] evaluated five methods for parameter calibration of J-C constitutive model, providing guidance for the determination of J-C parameters. Huang et al. [19] gave J-C constitutive and failure model parameters of 45 steel and TC4 steel. Pervaiz et al. [20] and Wang et al. [21] presented a finite element method (FEM) of Charpy impact, and provided schemes and suggestions for numerical simulation. Kim et al. [22] proposed a method to simulate the mixed fracture mode of ductile fracture and cleavage fracture, and experimentally verified it by using the Charpy test data of X80 steel. Furthermore, good consistency between theory and experiment was achieved from fracture morphology and impact energy. Fang and Ding [23], based on the force analysis, determined the load characteristic points according to the force-displacement curve with the instrumental Charpy impact tester. Force-based analysis method has become a new method to evaluate the dynamic fracture properties of materials, which makes up for the deficiency of traditional Charpy impact method. Therefore, it has become an important analysis tool to evaluate the dynamic fracture properties, and reveal their fracture mechanism.

There are many experiments and finite element simulation studies on Charpy impact, but there are still few studies on the influence of geometric factors such as side groove on Charpy impact through experiments and simulation. In this paper, the J-C model is used to simulate the impact behavior of pressure vessel steel in ABAQUS, and the influence of several important geometric factors on the impact behavior of materials is studied. It can provide reliable support for engineering practice.

2 Experimental and Theoretical Preparation

2.1 Charpy Impact Test

Charpy impact test is conducted according to GB/T 229-2020 and ASTM E23-2018. Standard V-notch specimens are adopted in the test, and the profile dimensions of the specimens adopt herein are the same. The test specimen is shown in Figure 1(a), and the geometric sizes are shown in Figure 1(b). The length of impact specimen is 55 mm, the width and height of which are 10 mm respectively. Figure 1(c) shows an instrumented Charpy impact tester. The notched specimen is placed between the two support blocks of the test machine, the notch is towards the impact surface. In order to measure the absorbed energy, the specimen is impacted with a pendulum. A force sensor at the bottom of the pendulum records the load-displacement curve during impact.

2.2 Theoretical Model

2.2.1 Johnson-Cook Constitutive Model

On the basis of continuous damage mechanics (CDM) and viscoplastic mechanics, Mao et al. [24] and Johnson et al. [25] comprehensively analyzed the effects of high strain rate, temperature and large deformation on the relationship of stress and strain. Furthermore, they proposed a classic constitutive model (named Johnson-Cook constitutive model). Besides, stress is expressed as the product of strain hardening term, strain rate hardening term, and thermal softening term. Finally, the specific form is descried as follows:

$$\sigma=\left(A+B\varepsilon^{n}\right)\left(1+C\ln\dot{\varepsilon}^{*}\right)\left[1-\left(T^{*}\right)^{m}\right], \tag{1}$$

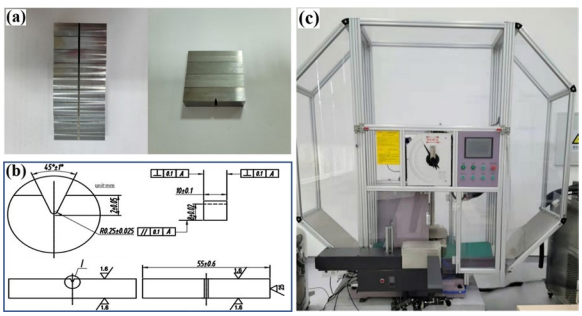

Figure 1 Impact testing system: (**a**) Charpy impact specimen, (**b**) Impact specimen dimensions, (**c**) Instrumented Charpy impact machine

$$\dot{\varepsilon}^* = \frac{\dot{\varepsilon}}{\dot{\varepsilon}_o}, \tag{2}$$

$$T^* = \frac{(T - T_r)}{(T_m - T_r)}. \tag{3}$$

In Eq. (1), A is the initial yield stress at the reference strain rate and temperature; B is the strain hardening modulus; C is the strain rate hardening parameter; n is the strain hardening index; m is the thermal softening index; $\dot{\varepsilon}^*$ is the plastic strain rate. In Eq. (3), T^* is dimensionless temperature term related to thermal softening; T is the working temperature, T_r is the room temperature, and T_m is the melting temperature of the material.

2.2.2 Johnson-Cook Failure Criteria

The fracture criterion firstly proposed by Johnson and Cook had been further developed by Portillo and Eduardo [26], which makes the fracture strain sensitive to stress triaxiality, temperature, and strain rate. The model assumes that during the plastic strain process, damage accumulates in the material element. When the critical value is reached, the plastic strain accelerates immediately up to final rupture. The failure model can be expressed as follows:

$$\varepsilon_f = \left(D_1 + D_2 e^{D_3 \sigma^*}\right)\left(1 + D_4 \ln \dot{\varepsilon}_q^*\right)\left(1 + D_5 T^*\right). \tag{4}$$

In Eq. (4), ε_f represents the current fracture strain that depends on the stress triaxiality, strain rate and temperature; D_1–D_5 are the material damage parameters, where D_1–D_3 are the parameters related to stress triaxiality, D_4 is the parameter related to strain rate, and D_5 is the parameter related to temperature, D_5 is negligible at room temperature. According to the relationship between the stress triaxiality and the fracture strain obtained by the tensile test on notched rod, parameters of D_1–D_3 can be fitted by the least squares fitting method. Besides, the parameter D_4 can be determined by comparing the load-displacement curve by test and the simulation one by FEM. Numerical simulations were performed using J-C model for 16MND5 steel, the parameters of which are shown in Table 1.

The J-C fracture criterion is based on the equivalent plastic strain at the element integration point. When the damage parameter D reaches 1, the material fails,

$$D = \sum \frac{\Delta \varepsilon^{pl}}{\varepsilon_f}. \tag{5}$$

In Eq. (5), $\Delta \varepsilon^{pl}$ is the equivalent plastic strain increment, and ε_f is the final fracture strain of the material.

2.2.3 Finite Element Modeling

The numerical simulation of Charpy impact was carried out with ABAQUS software, and the specimen of the 3D deformable body was established. The FEM includes the impact pendulum and the specimen support. Actually, the fracture of the sample is caused by the collision between the pendulum and the specimen. For the convenience of calculation, the pendulum is simplified as a rigid body, and the specific model is shown in Figure 2(a). The material of the punch and support is defined as an analytical rigid body. The material density is 7.8×10^3 kg/m^3, the elastic modulus is 205 GPa, and the Poisson's ratio is 0.3. The pre-defined initial velocity of the punch is set to 5.23 m/s along the Y-axis, while constraining the movement in the remaining directions. For the sample support, all directions are constrained, whereas the sample is not constrained. For the punch and the sample, the motion contact is set between the sample and the support, and the friction coefficient is 0.2 [27]. The mesh

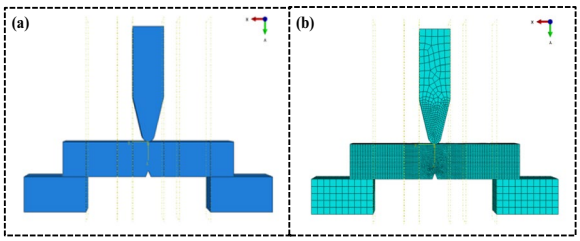

Figure 2 Front view of impact specimen in clamping state: (**a**) Geometric model, (**b**) Mesh division pattern

Table 1 J-C constitutive model parameters of 16MND5 steel

Material	P (kg·m^{-1})	E (GPa)	u	A (MPa)	B (MPa)
16MND5	7800	205	0.3	445.2	899.7
n	c	m	D_1	D_2	D_3
0.52	0.039	0.152	0.20	0.587	1.677
D_4	D_5				
0.005	−0.857				

division is shown in Figure 2(b), the mesh is refined at the contact position on the sample. The seed density is 0.2, the rest of which is 0.8; the seed density of the punch is 0.3 near the contact region, while the support has a seed density of 2. The element type is set to C3D8R (8-node hexahedral reduced-integration solid element (hourglass control)). The total number of grids is 298000 and the total number of nodes is 312273. In simulation, the entire impact time is set to 0.005 s.

3 Results and Discussion

In fact, there are many factors that affect the results of Charpy impact test, and sometimes the result data may have great discreteness, and even error. These factors include sample size, notch type, side groove and other geometric factors; also includes impact speed, temperature, pendulum size and other test conditions. In order to study the influence of geometric dimension factors on Charpy impact test, the related test was carried out first, then the FEM was verified and validated, and finally the impact behavior was fully analyzed by using the verified FEM with the calibrated parameters.

Charpy impact energy is the traditional parameter to evaluate the toughness of materials, but the single parameter evaluation has great shortcomings. The load-displacement curve can be obtained by instrumented Charpy impact test. By analyzing the parameters of each characteristic area of the curve, the deficiency of single parameter method can be overcome, and accurate toughness properties can be obtained. The traditional Charpy impact test is completed by a single impact on the stress-concentrated specimen. The impact curve is shown in Figure 3. The area enclosed by the curve is the impact energy, which can be divided into four parts: The first part is the elastic work E_e consumed in elastic deformation; the second part is the plastic work E_P consumed in plastic deformation until the initial crack; the third part is the tear work E_T consumed by crack initiation, propagation and fracture; the fourth part is the crack stopping energy E_B. Among the four parameters, the plastic work E_p and the tear work E_T reflect the anti-fracture ability of the material. E_p reflects the ability to resist plastic deformation, and E_T reflects the ability to resist fracture. Therefore, only the crack propagation work can truly reflect the toughness of the material. In other words, the impact toughness of the material is determined by the crack propagation energy, so it is scientific and reasonable for the force-displacement curve to reflect the toughness of materials. F_m is the maximum load in the test process, F_{gy} is the yield load of the test, and F_{iu} is the load when the crack reaches the critical length, and at that time the instability propagation occurs.

3.1 Charpy Impact Simulation and Validation

Figure 4 shows the comparison between the numerical simulation and the experimental test for the force vs. displacement, and also for absorbed energy vs. displacement curves in Charpy impact. It can be seen from Figure 4 that the simulated curves are basically consistent with the experimental ones. Analyzing the maximum force and impact energy of Charpy impact, it can be seen that the maximum impact force is 18.3 kN; while the simulated one of impact energy is 35 J lower than the experimental one, and the error between the two is within 20%, which meets the accuracy required in engineering application. As for the source of this error, the impact energy of the test represents the difference between the initial kinetic energy and the kinetic energy when the pendulum reaches the lowest point. This energy includes the impact

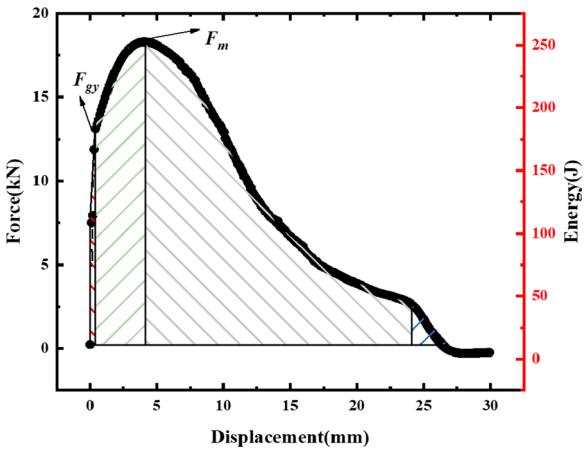

Figure 3 Schematic diagram of energy division of Charpy impact curve

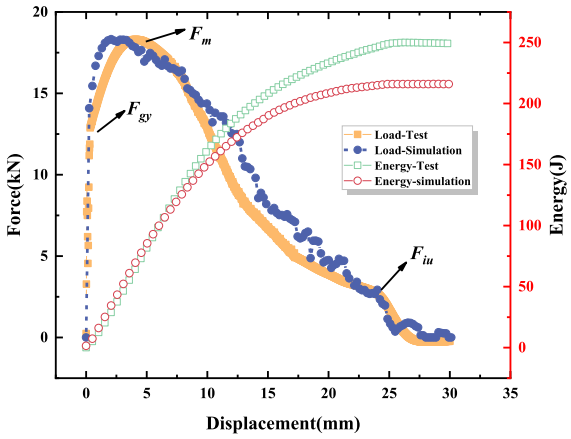

Figure 4 Comparison of simulation and experimental for both force vs. displacement and energy vs. displacement curves of Charpy impact

energy of the material, the viscous dissipation energy and friction dissipation energy of the impact process. These energies are dissipated in the form of heat energy, so the impact energy of the test is actually greater than the energy used by the material for cracking. This leads to the deviation between the numerical calculation and the experimental results. This part is the main source of error.

From the comparison of simulation and test in Figure 4, it can be seen that the model and calculation results used for the 16MND5 steel can describe the impact behavior during the entire test process. It is worth noting that the analysis for the force vs. displacement curve is obtained on the force-based analysis method (FBA), which is consistent with the method used in Ref. [28].

Figure 5 shows the macroscopic fracture morphology for Charpy impact, which is mainly divided into four regions: (1) The first part is the crack source region. The specimen notch root is mainly affected by the tensile stress during the impact, crack initiates at the middle of the root or slightly from the notch surface, including elastic zone and plastic zone, whose impact energy corresponding to E_e and E_p respectively. (2) The second part is the fibrous zone, which is the steady-state propagation area of the crack along both sides and depth direction, generally showing gray fracture morphology [14]. It is corresponding to stable propagation stage in load-displacement curve, and the corresponding energy is E_T. (3) The third part is the radial zone. When the cracks in the fibrous zone grow up to the critical crack size, the cracks begin to propagate unstably, and have the radial characteristics. The fracture morphology shows the radial morphology with the fibrous zone as the center. This load-displacement curve corresponds to the instable fracture stage, and the corresponding energy is E_B. (4) The fourth part is the shear-lip region, which is the characteristic region formed in the last stage of fracture.

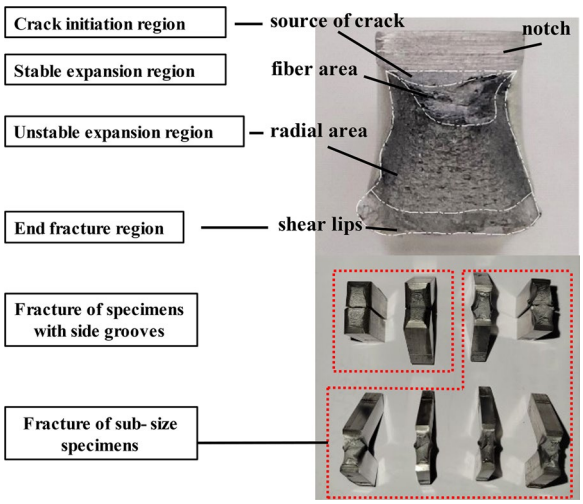

Figure 5 Charpy impact fracture morphology and characteristic area

3.2 Effect of the Specimen Width

In practice, parts with small cross-sectional thicknesses or complex shapes are difficult to process into standard full-size (10 mm×10 mm×55 mm) Charpy V-notch specimens. In such cases, specimens with reduced width can be selected for processing and testing. Typical sizes of small specimen width are 7.5 mm (3/4 size), 6.67 mm (2/3 size), 5 mm (1/2 size), 3.33 (1/3 size) and 2.5 mm (1/4 size). The initial velocity of the pendulum was set to 5.23 m/s. Charpy impacts were simulated for the specimen with 7.5 mm and 5 mm in this paper, and the results are shown in Figures 6 and 7.

Figure 6 shows the effect of specimen width on impact residual velocity. It can be seen in Figure 6 that, as the

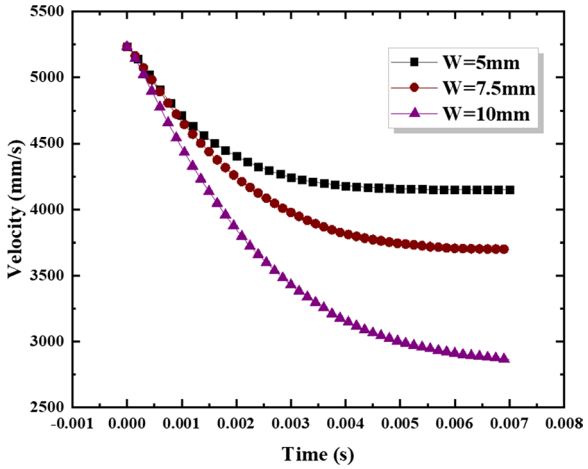

Figure 6 Effect of specimen width on impact residual velocity

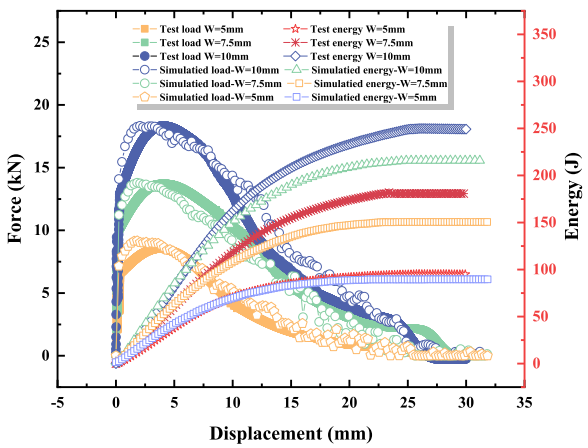

Figure 7 Influence of specimen width on impact force and absorbed energy vs. displacement curves

impact time increases, the pendulum speed experiences a rapid decrease to a slow decrease, and finally down to a lower residual speed. This is because during the impact test, the kinetic energy of the pendulum is converted into the absorbed energy of the specimen plus the energy of crack propagation. The specimen absorbs a large impact kinetic energy at the initial stage of the impact, and then absorbs a smaller impact kinetic energy at the stage of stable crack propagation. Thus, the difference between the kinetic energy before and after the impact can be defined as the impact energy of the specimen. Further from Figure 4, it can be seen that as the width of the specimen increases, the residual velocity of the pendulum decreases, and the time for the specimen to be knocked out of the bracket increases, which indicates that the specimen with smaller width absorbs less energy, which is consistent with the following test and simulation results in Figure 7.

Figure 7 shows the comparison between test and simulation results of force vs. displacement curves of Charpy impact under different widths. The area surrounded by the curve in Figure 7 is the impact absorption energy of the specimen. The impact energy and maximum impact force are shown in Table 2. In terms of impact energy, the simulated result is slightly different from the experimental one, but it can meet the requirements of engineering application. The experimental one of maximum impact force is basically consistent with the simulated one, the simulation of force and energy vs. displacement curves during the impact process in Figure 7 is consistent with the experimental ones, which can reflect the evolution of the whole impact behavior well.

The test results of impact force and absorption energy are also shown in Figure 7. It can be seen from Figure 7 that the width of the specimen has an inlfuence on the impact result as follows: With the increase of the width, the maximum displacement of the specimen at fracture is basically the same, about 30 mm. The maximum impact force increases with the increase of the width, and for the specimen with half of the standard width, the maximum impact force is 8.53 kN; for 3/4 standard width specimen, the maximum impact force is 13.72 kN; for the full size one, the maximum impact force is 18.3 kN. The maximum impact force is positively correlated with specimen width. For the specimen with the corresponding width above, the impact energy are 95.0 J, 190.2 J and 249.2 J respectively, which is also positively correlated with the specimen width.

Table 2 Theoretical and experimental data of maximum impact force and absorbed energy with different widths

Specimen width (mm)	5	7.5	10
Energy from test (J)	95	190.2	249.2
Energy from simulation (J)	89.5	155.5	215.9
F_m from test (kN)	8.53	13.72	18.3
F_m from simulation (kN)	9	13.8	18.3

Figures 8 and 9 respectively show the proportion distribution of characteristic regions of test and simulated impact energy. The steady-state crack propagation energy E_T represents the toughness of the material, and the proportion of E_T to the whole impact energy should be concerned. The ratio of E_T to the whole impact energy is 70.603% for the specimen with 5 mm width, while the simulated one is 74.942%. The ratio of E_T to the whole impact energy is 75.126% for the specimen with 7.5 mm width, while the simulated one is 76.925%. The ratio of E_T to the whole impact energy is 72.478% for the specimen with 10 mm width, while the simulated one is 74.843%. In general, the width of specimen has slight influence on steady-state propagation energy, and the proportion variation of E_T to the whole impact energy is very small. Moreover, the steady-state propagation energy of

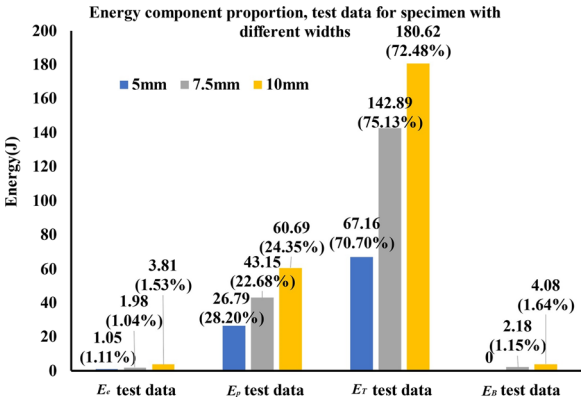

Figure 8 Energy component proportion distribution diagram of impact specimen with different widths in Charpy impact test

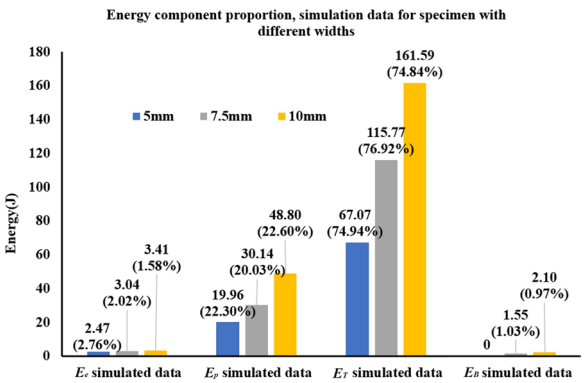

Figure 9 Energy component proportion distribution diagram of impact specimen with different widths in Charpy impact simulation

specimen with different sizes is about 70%−75%, and the simulation results are basically consistent with the measured ones. The plastic work E_p represents the ability of material to resist plastic deformation, and the proportion of E_p to the whole impact energy is between 22%−28% in the test. The percentage of E_p to the whole impact energy in the simulation ranged from 20% to 22%, which was in agreement with the test.

3.3 Effect of the Side Groove Depth

The ASTM E23-2018 standard [29] specifies a maximum depth of 0.25 times the thickness for side grooves. Accordingly, the maximum depth of 2.5 mm is set for the specimen with a width of 10 mm. Two side grooves were machined on both sides of the notch for specimen in order to study the impact performance for the specimen with the side grooves. The specific processing size is shown in Figure 10.

Charpy impact of specimens with side groove depth of 1 mm, 1.5 mm, 2 mm and 2.5 mm were simulated, and the influence of side groove depth on impact behavior was analyzed. The simulation results are shown in Figures 11, 12, 13, 14. Clearly, Figure 11 shows the comparison between the impact simulation and the test results of the side groove specimen. The fracture morphology and side expansion pattern of the two are consistent. Figure 12 shows the comparison of the load vs. displacement curves between the test and simulation for the specimen with 2 mm side groove. The curves are close to each other, the maximum load difference is less than 3 kN, the impact energy difference is 8 J, the error is about 8.8%. Figure 13 shows the impact simulation results of specimen with different side groove depths. It can be seen from Figure 13 that the existence of side groove reduces the maximum impact force, reduces the overall impact energy, and shortens the impact time. The maximum impact force of the specimen without side groove is

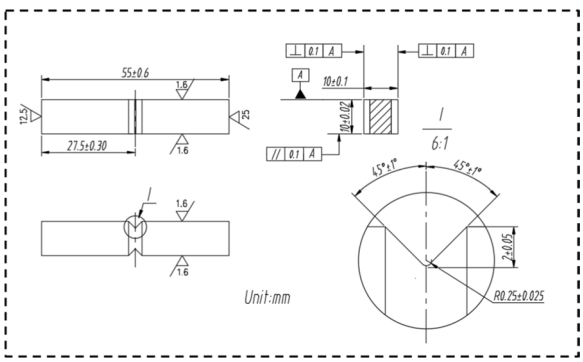

Figure 10 Dimension description of Charpy impact specimen with 2 mm side groove

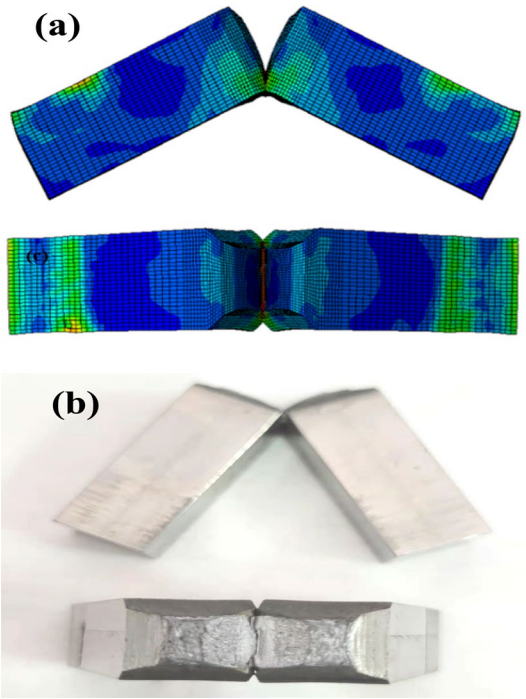

Figure 11 Fractured surface morphology: (**a**) Fractographic features in simulation, (**b**) Fractographic features in test

18.3 kN, and the maximum impact force of the specimen with 2 mm side groove depth is 16.0 kN. When the specimen depth is 2 mm, the impact absorption energy decreases from 215.9 J without side grooves to 80.04 J with side grooves.

In general, there is a negative correlation between the side groove size and the maximum impact force, that is, the greater the depth of side groove, the smaller the

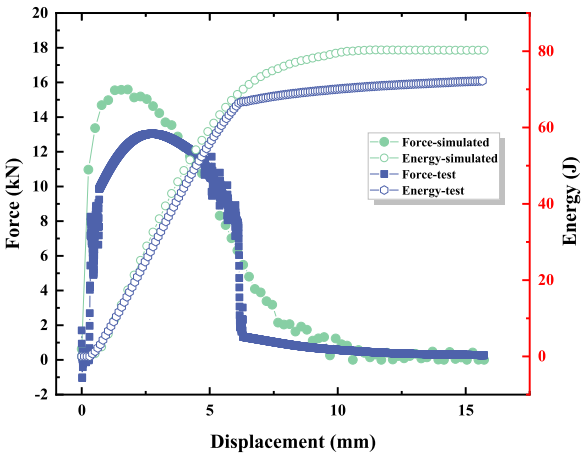

Figure 12 Test and simulation curves of impact energy and force vs. displacement for the specimen with side groove

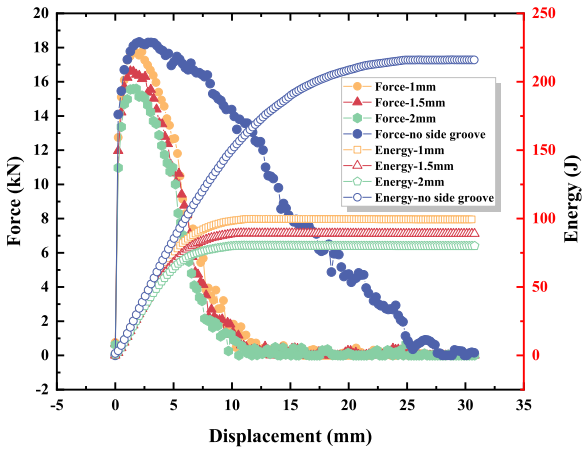

Figure 13 Influence of side groove depth on impact force vs. displacement and absorbed energy vs. displacement curves

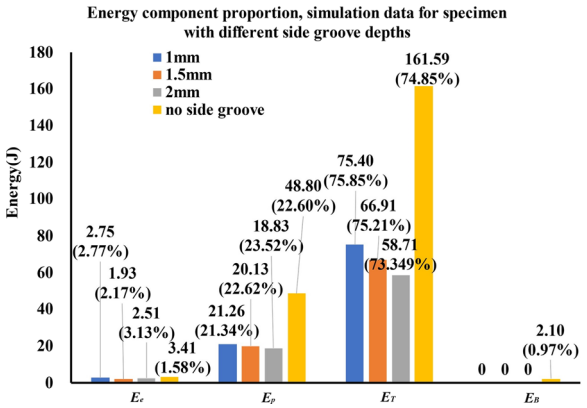

Figure 14 Energy component proportion distribution diagram of impact specimen with different side grooves during impact process

maximum impact force. The reason may be that the increase of the depth of the side groove leads to the decrease of the elements that can resist the crack propagation near the notch, therefore the crack propagation is easier. In other words, the decrease of the geometric constraint leads to the faster crack propagation.

The fracture displacement of the specimen without side groove is 25 mm, and that of the specimen with side groove is 10 mm. By comparing the curves in Figure 13, it can be seen that the existence of side grooves reduce the fracture displacement of materials. It is found that the depth of side grooves has almost no effect on the fracture displacement, and the fracture displacement is almost 10 mm. Figure 13 reveals that the existence of side grooves accelerates the crack propagation near the side grooves, and the energy required for crack propagation is reduced, making the crack propagation easier.

As shown in Figure 14, for the impact specimen with different side groove, energy percentage sited in the characteristic regions has some changes. The overall impact energy decrease, but the percentage of tearing energy and plasticity energy are still around 75% and 22% respectively, which is basically consistent with the results for the specimen without side grooves. It can be inferred that the side groove effect is insignificant on plasticity energy for this material during the impact process.

3.4 Effect of the Side Groove Angle

As shown in Figure 15, the standard side grooves are V-shaped side grooves processed on the surface of both sides of the specimen along the length of the notch, with a depth of 2 mm and an angle of 90°. In order to study the influence of side groove angle on impact behaviors, the simulation is performed by adopting the angles of 60°, 70°, 80°, 90°, 100°, the results of which are shown in Figure 15. As can be seen, different side groove angles have little influence on the force-displacement curve. They are basically consistent with each other, so the impact absorption energy is basically the same, about 85.1 J. Generally speaking, the influence of side groove angle on impact behavior can be ignored.

3.5 Effect of the Side Groove Fillet

The thinest wired-cut molybdenum wire also has some thickness, so there must be a rounded corner in the processing of side grooves in specimen. The rounded corner form of side groove is shown in Figure 10. Therefore, it is necessary to study the effect of fillet size on impact behavior. Finite element models of different fillet sizes (R = 0.1 mm; 0.25 mm; 0.4 mm; 0.5 mm) were established, and the simulation results on impact behavior of different side groove fillets are shown in Figure 16.

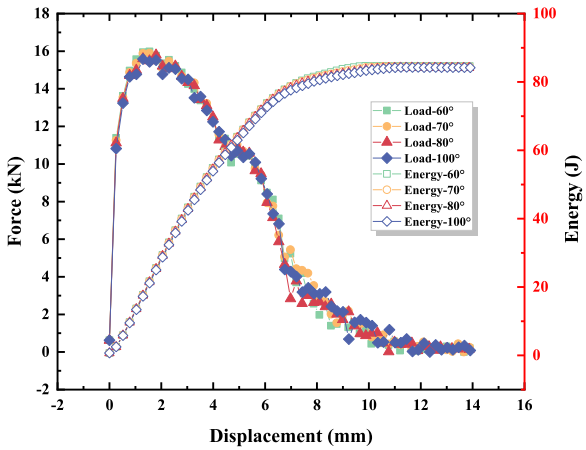

Figure 15 Influence of side groove angle on the curves of force vs. displacement and energy vs. displacement

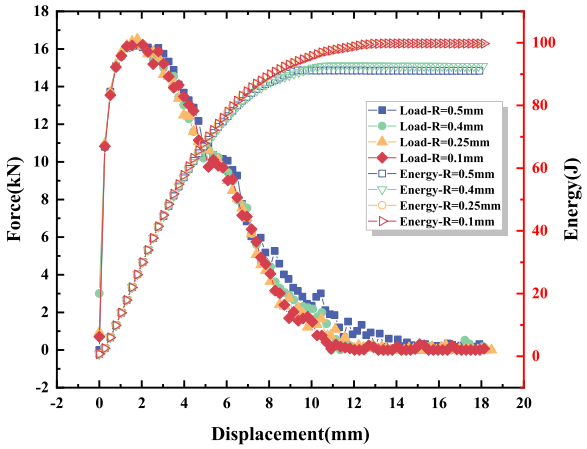

Figure 16 Effect of the side groove fillet on the curves of force vs. displacement and energy vs. displacement

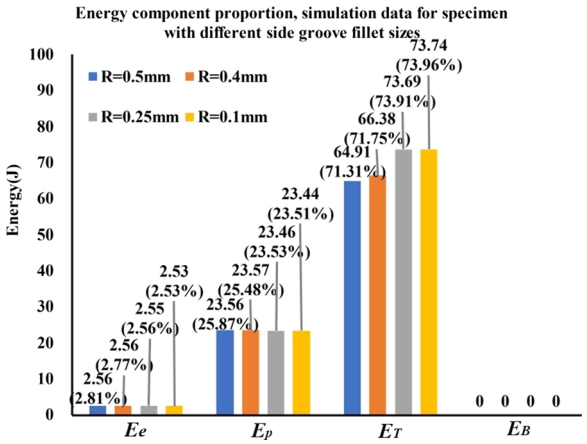

Figure 17 Energy component proportion distribution diagram of impact specimen with different fillet radius during impact process

As can be seen from Figure 16, when the side groove fillet is 0.1 mm, the maximum impact force is 16.8 kN, and the absorbed energy is 100.5 J. When the fillet is 0.25 mm, the maximum impact force is 16.8 kN, and the absorption energy is 99.5 J. When the fillet is 0.4 mm, the maximum impact force is 16.3 kN, and the absorption energy is 93.2 J. When the fillet is 0.5 mm, the maximum impact force is 16.1 kN, and the absorbed energy is 90.5 J. Figure 16 discloses that the size of side groove fillet is positively correlated with absorption energy, but has little relationship with maximum impact force. Clearly, the larger the side groove fillet is, the larger area enclosed by the force vs. displacement curve, indicating that the larger the absorbed energy is. Overall, the different side groove fillets caused nearly 10% variation in the absorbed energy.

By analyzing the energy distribution of the curve in Figure 17, it can be seen that the fillet radius at the side groove root mainly affects the tearing energy. Furthermore, the larger the fillet is, the smaller the tearing energy is, and the lower the toughness is. The percentage of tear energy and plastic energy are about 72% and 24% respectively.

3.6 Effect of the Side Groove on the Stress Triaxiality

To investigate the relationship between different stress states and fracture mechanisms, stress trixiality are often introduced to describe different stress states [30, 31], which is defined as follows:

$$R_\sigma = \frac{\sigma_m}{\sigma_{eq}}. \tag{6}$$

From the definition of stress triaxiality, it can be seen that stress triaxiality is the ratio of hydrostatic stress to Mises equivalent stress. The hydrostatic stress causes volume change, while the Mises equivalent stress reflects the shape change. Stress triaxiality is used as a parameter to describe the stress state, which also reflects volume change and shape change. When the stress triaxiality is negative, the structure is in compression, while the stress triaxiality is positive, the structure is in tension. In this paper, specimens with different side groove fillets were simulated to analyze the effect of side groove fillet on stress triaxiality, the results of which are shown in Figures 18 and 19.

During the simulated impact, the triaxiality of each element at the bottom of the V-notch was extracted when t = 0.0001 s (before the first element failure). Using the distance between each element and the side surface as the horizontal coordinate and the triaxiality of the element as the vertical coordinate, the triaxiality of each element is plotted. The results are shown in Figure 19. The triaxiality of the units on both sides of the specimen is significantly smaller than that of the middle part. The triaxiality of the elements on both sides is about 1.0. The triaxiality increases with the increase of the fillet angle of the side grooves.

It can be seen from Figure 19 that the maximum triaxiality of impact specimens without side groove is 1.05, showing flat form along the crack front. The maximum triaxiality of the specimen with side groove is 1.4, which appears in the middle part of the crack. It is worth noting that the triaxiality fluctuation appears in the specimen without side grooves near the free surfaces of both sides, while the triaxiality factor fluctuation does not appear in the specimen with side grooves during impact. The above phenomenon shows that the intermediate element first fails and then expands to both sides in the fracture process.

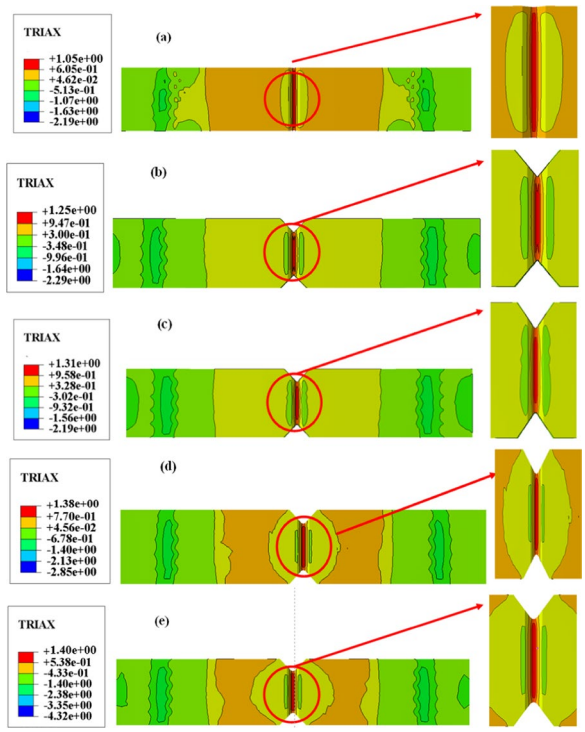

Figure 18 Triaxiality distribution among impact specimen (**a**) without side groove, with side groove fillet of (**b**) R = 0.1 mm, (**c**) 0.25 mm, (**d**) 0.4 mm, (**e**) 0.5 mm

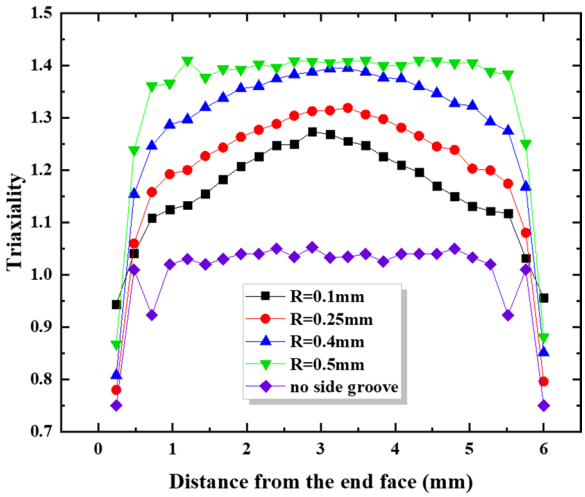

Figure 19 Triaxiality distribution of different impact specimens along the crack front

4 Conclusions

(1) The influence of side grooves and width of specimen on Charpy impact behavior is studied by experiment and numerical simulation. The existence of side grooves greatly reduces the impact force and impact energy, accelerates the crack propagation, and leads to more straight fracture surface. The side groove depth has great influence on Charpy impact. Maximum force and impact energy decrease as depth increases. But side groove angle has little effect on impact performance. The side groove fillet has a slight influence on the impact absorption energy, impact absorption energy increases with the decrease of fillet radius. As for the influence of width on impact energy, the impact energy increases with the increase of specimen width.

(2) In the crack initiation stage, the existence of side grooves leads to the increase of stress triaxiality of elements. The larger the side groove fillet is, the greater the stress triaxiality is, and the more elements in the width direction of the specimen reach the maximum stress triaxiality. Therefore, the impact specimen with side groove first cracks from the middle position of the width, and then expands to both sides.

(3) After energy partition analysis of impact curve, the proportion of tearing energy and plastic energy is slightly affected by specimen width and side groove size for 16MND5 steel. In general, tearing energy approximately accounts for 72%, and plastic energy for 24%.

(4) The results reveal the influence of side grooves and specimen width on the impact absorbed energy of specimens, which can provide a reference for the design of solutions for impact toughness determination of high toughness materials.

Acknowledgements

The authors sincerely thanks to professor Yanguo Zhou, and Shandong Tu of *East China University of Science and Technology* for their critical discussion and reading during manuscript preparation.

Authors' Contributions

JM puted forward the test method, reviewed and edited the first draft, verified the rationality of the results, provided funds, supervised the whole work and carried out project management; QX was responsible for finite element simulation and results analysis; JY was responsible for proposing experimental ideas, realizing the whole experiment and numerical simulation, as well as data collation and writing the first draft; CC was mainly responsible for assisting sampling and analysis, and DW provided test materials; FZ provided test instruments and equipment management; MC was mainly responsible for resource and method discussion; All authors read and approved the final manuscript.

Authors' Information

Jianfeng Mao, born in 1983, graduated from *Shanghai Jiao Tong University, China* (Ph.D.), and is now a doctoral supervisor and associate researcher at *School of Mechanical Engineering, Zhejiang University of Technology, China*. He is engaged in teaching and scientific research of structural integrity technology.

Qian Xu, born in 2000, is currently a master degree candidate at *Zhejiang University of Technology, China*. His main research interest is structural integrity technology.

Jiadong Yang, born in 1998, obtained master's degree in energy and power from *Zhejiang University of Technology, China*. His main research interest is structural integrity technology.

Chi Cao, born in 2000, is currently a master degree candidate at *Zhejiang University of Technology, China*. His main research interests is strength of nuclear power materials.

Dasheng Wang born in 1986, obtained master's degree in engineering mechanics from *Harbin Institute of Technology, China*. His main research interest is strength of nuclear power structure.
Fengping Zhong born in 1973, obtained master's degree in chemical machine from *Zhejiang University, China*. His main research interest is pressure vessel inspection technology.
Mingya Chen born in 1985, obtained Ph.D. degree in chemical machine from *Shandong University, China*. His main research interest is safety evaluation of nuclear power pressure equipment.

Funding
Supported by National Natural Science Foundation of China (Grant Nos. 51975526, 51505425), National Key R&D Program of China (Grant No. 2018YFC0808800), Open Project of Key Laboratory of MEM of China (Grant No. 2020XFZB10), Technical Service Projects (Grant Nos. HZFS-XZ-2022-07-02, XJBY-20211221).

Data availability
Data in the paper can be provided upon reasonable requirement.

Declarations

Competing Interests
The authors declare no competing financial interests.

Received: 25 February 2022 Revised: 24 November 2023 Accepted: 30 November 2023
Published online: 03 January 2024

References

[1] X D Chen, Z C Fan, J Cui, et al. Progress in high-performance manufacturing technology for pressure vessels in China. *Pressure Vessel Technology*, 2021, 38(10) : 1–15
[2] J Zhu, D S Wang, S Y Bao, et al. Experimental and numerical study on multiaxial creep behavior of 16MND5 steel at 700℃. *Journal of Nuclear Materials*, 2021, 558: 153387.
[3] J F Mao, X Y Li, D S Wang, et al. Experimental study on creep-fatigue behaviors of Chinese P92 steel with consideration of several important factors. *International Journal of Fatigue*, 2021, 142: 105900.
[4] J F Mao, J D Yang, J Zhu, et al. Experimental and theoretical research on creep-fatigue behaviors of 316L steel with and without 650℃ thermal aging. *Fatigue & Fracture of Engineering Materials & Structures*, 2022, 45: 1179–1198.
[5] Z H Liu, X Wang, X Chen. Fracture performance and prediction of RPV structural steels related to in-plane and out-of-plane constraints. *Pressure Vessel Technology*, 2021, 38(11): 1–8.
[6] L L Gui, X X Shang, K Liu, et al. Determination of minimum allowable service temperature of X80 pipeline steel based on fracture mechanics. *Pressure Vessel Technology*, 2021, 38(9): 40–45.
[7] J B Zhang, S H Liu, Y Gu. Effect of PWHT on impact property and fracture toughness of SA 738 Gr.B steel heat affected zone. *Pressure Vessel Technology*, 2021, 38(8): 29–33.
[8] R Johnson, W K Cook. A constitutive model and data for metals subjected to large strains high strain rates and high temperatures. *The 7th International Symposium on Ballistics*. 1983, 21: 541–548.
[9] W P Lin, N Li, H J Zhang, et al. Influencing factors of two kinds of tubular goods' Charpy impact test. *Petroleum Tubular Goods & Instruments*, 2019, 5(6): 16–18.
[10] G Terán, S Capula-Colindres, F Chávez, et al. Charpy impact toughness in all directions with respect to the rolling direction of API 5L X52 pipeline steel. *MRS Advances*, 2022: 2059–8521.
[11] F D Gioacchino, E Lucon, E B Mitchell, et al. Side-grooved charpy impact testing: Assessment of splitting and fracture properties of high-toughness plate steels. *Engineering Fracture Mechanics*, 2021: 107842.
[12] E Lucon. Cost-effective alternatives to conventional Charpy tests for measuring the impact toughness of very-high-toughness steels. *Journal of Pressure Vessel Technology*, 2018, 140(2): 021401.
[13] H M Al-Jabr, D K Matlock, J G Speer. Modified impact testing method to evaluate toughness of higher API grades. *2rd International Symposium on the Recent Developments in Plate Steels, AIST*, 2018: 253–261.
[14] E Kondryakov, O Panasenko, A Kravchyk, et al. Peculiarities of the crack initiation and propagation in different specimen types. *Procedia Structural Integrity*, 2019: 43–50.
[15] E A Kondryakov, A V Panasenko, V V Kharchenko. Experimental determination of the moment of fracture initiation in standard Charpy specimens and specimens with edge notches. *Strength of Materials*, 2015(47): 291–6.
[16] A Banerjee, S Dhar, S Acharyya, et al. Determination of Johnson cook material and failure model constants and numerical modelling of Charpy impact test of armour steel. *Materials Science & Engineering A*, 2015, 640(29): 200–209.
[17] Y Cao, Y Zhen, M Song, et al. Determination of Johnson–Cook parameters and evaluation of Charpy impact test performance for X80 pipeline steel. *International Journal of Mechanical Sciences*, 2020, 179(45): 105627.
[18] L Gambirasio, E Rizzi. On the calibration strategies of the Johnson–Cook strength model: discussion and applications to experimental data. *Materials Science and Engineering: A* , 2014, 610: 370–413.
[19] T Huang, W G Wu, X B Li, et al. Numerical investigation on truncated cylindroconical projectile penetrating thin target. *Chinese Journal of Ship Research*, 2009, 4(2): 48–52.
[20] S Pervaiz, S Kannan, K Ram, et al. Numerical modeling of Charpy impact test to determine the fracture characteristics of aluminium alloy 6061. *Fracture, Fatigue, Failure and Damage Evolution*, 2019(6): 85–88.
[21] T Y Wang, Y D Wang, H Y Wang, et al. Finite element modeling for Charpy impact test of Q345R. *Process Equipment & Piping*, 2013, 50(6): 10–14.
[22] J S Kim, Y J Kim, M W Lee, et al. Fracture simulation model for API X80 Charpy test in Ductile-Brittle transition temperatures. *International Journal of Mechanical Sciences*, 2020, 182: 105771.
[23] J Fang, F L Ding. Force based analysis by using instrumented Charpy impact. *Journal of Mechanical Strength*, 2004, (s1): 291–294.
[24] J F Mao, W Z Wang, J H Zhang, et al. Numerical investigation on the dynamic behaviors of turbine valve disc–seat impact at low velocity. *Journal of Mechanical Science and Technology*, 2015, 29(2): 507–515.
[25] G R Johnson, W H Cook. Fracture characteristics of three metals subjected to various strains, strain rates, temperatures and pressures. *Engineering Fracture Mechanics*, 1985, 21(1): 31–48.
[26] O Portillo, R L Eduardo. Impact performance of advanced high strength steel thin-walled columns. *Proceedings of the World Congress on Engineering*, 2008, 2: 1331–1336.
[27] Y Lin, W Yang, Z Tong. Charpy impact test on A508-3 steel after neutron irradiation. *Engineering Failure Analysis*, 2017, 82: 733–740.
[28] The World Trade Organization Technical Committee, American National Standard. ASTM E23-18 Standard test methods for notched bar impact testing of metallic materials. New York: American National Standard Publishing House, 2018.
[29] J R Rice, D M Tracey. On the ductile enlargement of voids in triaxial stress fields. *Journal of the Mechanics and Physics of Solids*, 1969, 17(3): 201–17.
[30] A Y Liao, J Zhu, J F Mao, et al. Characterization of multiaxial creep behaviors of 16MND5 steel at pre- and post-phase transformation. *Journal of Materials Engineering and Performance*, 2023, 23: 08635–5.
[31] J F Mao, C Cao, J D Yang, et al. Research on multi-scale failure mechanism of gradient nanostructured 316L steel under strain-controlled fatigue at 650℃. *International Journal of Fatigue*, 2023, 177:107970.